Research Article

Subramanian Mohanaparameswari, Manavalan Balachandramohan*, Ponnusamy Sasikumar*, Chinnaiyan Rajeevgandhi, Mark Vimalan*, Sanmugam Pugazhendhi, Krishnamurthy Ganesh Kumar, Salim Albukhaty*, Ghassan M. Sulaiman, Mosleh M. Abomughaid, and Mohammed Abu-Alghayth

Investigation of structural properties and antibacterial activity of AgO nanoparticle extract from *Solanum nigrum/Mentha* leaf extracts by green synthesis method

https://doi.org/10.1515/gps-2023-0080
received May 28, 2023; accepted October 9, 2023

Abstract: *Solanum nigrum* and *Mentha* leaf extracts were used as reducing and stabilizing reagents in the green synthesis of silver oxide nanoparticles (AgO NPs), and their antibacterial efficacy was subsequently evaluated. The structure and morphology of AgO NPs were evaluated using X-ray diffraction and filed emission scanning electron microscope. High-resolution transmission electron microscopy images were used to analyze the characteristics of certain particles with clearly discernible atomic structures. The functional group and elemental composition of AgO NPs were investigated using fourier transform infrared spectroscopy and energy dispersive X-ray spectroscopy. Ultraviolet–visible spectroscopy was used to determine the energy band gap (E_g) of the sample. The dielectric constant of both samples was found to be inversely proportional to frequency, whereas the dielectric loss was found to be directly proportional to temperature but directly proportional to frequency. This suggests that the space charge has an effect on the mechanism of charge transfer as well as polarizability. AC conductivity rises and is inversely proportional to temperature increases. AgO NPs had a size range of around 56 nm and were mostly spherical. The antibacterial potential of the synthesized AgO NPs using both extracts was compared by the well-diffusion method. AgO NPs at 50–100 $\mu g \cdot mL^{-1}$ concentration significantly inhibited the bacterial growth of *Bacillus cereus*, *Staphylococcus aureus*, *Escherichia coli*, and *Klebsiella pneumonia*.

Keywords: silver nanoparticles, *Solanum nigrum*, *Mentha*, green synthesis, structural properties

*** Corresponding author: Manavalan Balachandramohan**, Department of Physics, Erode Arts and Science College (Autonomous), Erode-638009, Tamilnadu, India, e-mail: balamohan2006@gmail.com
*** Corresponding author: Ponnusamy Sasikumar**, Department of Physics, Saveetha School of Engineering, SIMATS, Thandalam-602 105, Chennai, India, e-mail: sasijanaki123@gmail.com
*** Corresponding author: Mark Vimalan**, Department of Physics, Saveetha School of Engineering, SIMATS, Thandalam-602 105, Chennai, India, e-mail: myresearch1121@gmail.com
*** Corresponding author: Salim Albukhaty**, Department of Chemistry, College of Science, University of Misan, Maysan 62001, Iraq, e-mail: albukhaty.salim@uomisan.edu.iq
Subramanian Mohanaparameswari: Department of Physics, Erode Arts and Science College (Autonomous), Erode-638009, Tamilnadu, India
Chinnaiyan Rajeevgandhi, Sanmugam Pugazhendhi, Krishnamurthy Ganesh Kumar: Department of Physics, Saveetha School of Engineering, SIMATS, Thandalam-602 105, Chennai, India
Ghassan M. Sulaiman: Division of Biotechnology, Department of Applied Sciences, University of Technology, Baghdad 10066, Iraq
Mosleh M. Abomughaid: Department of Medical Laboratory Sciences, College of Applied Medical Sciences, University of Bisha, Al Nakhil, 255, Bisha 67714, Saudi Arabia
Mohammed Abu-Alghayth: Department of Clinical Laboratory Sciences, Faculty of Applied Medical Sciences, University of Bisha, 255, Al Nakhil, Bisha 67714, Saudi Arabia

1 Introduction

Herbal extract synthesis of metallic nanoparticles (NPs) generated considerable interest in the dynasty of nanotechnology due to its cost-effective method of producing NPs in lofty quality and quantity with minimal time use and a decrease in toxicity levels – in the case of drug delivery – compared to chemical synthesis, which uses harmful chemicals with high consumption and sensitive to the environment [1–3]. The field of nanotechnology has made amazing advances; however, researchers are turning to green metallic NPs to meet the need for ecologically friendly NP synthesis [4,5]. Metallic NPs from the green

synthesis clan can act as a capping and reducing agent [6,7]. A considerable amount of studies have systematically investigated metal nanostructures because of their unique catalytic, electrical, and optical capabilities [8]. In the province of metallic NPs, silver NPs fascinated the thoughts of researchers because of their idiosyncratic complexion in sensing, optoelectronic, catalysis, and drug delivery [9,10], and because of this, it is deemed that the production of silver NPs is of 500 tons every year and it may upswing in upcoming years [11]. Additionally, its significant contributions to the fields of high-sensitivity biomolecular detection, catalysis, medicine, and biosensors have suggested that it has inhibitory and bactericidal effects in combination with anti-angiogenesis, anti-inflammatory, and anti-fungal activities [12,13]. Significantly, silver oxide NPs (AgO NPs) have unique physical and chemical properties that are claimed to have great potential in medical applications. It can be non-toxic and environmentally friendly and reduce their size. NPs made using green synthesis are easier, more affordable, and more easily repeatable than those made using conventional techniques [14]. The heterogeneous fashion of green synthesis includes microorganisms that give the formation of NPs but the pace of synthesis is sluggish collated to routes involving an herbal course of action and relatively reincarnated and habitually aggregates in more anchored materials [15]. A large number of disease-causing water and foodborne pathogenic bacteria are actively engaged in the antibacterial action of the silver NPs [16]. *Solanum nigrum* and *Mentha* are significant homeopathic plants. *Solanum nigrum* and *Mentha* contain leaves that have rich amounts of calcium and minerals. The alkaloids and carbohydrates of the plant have a potent immune-stimulating impact. This was used to synthesize AgO NPs because it has anti-inflammatory and antibacterial effects [17]. This herb is used to treat the common cold and cough and is used in the Siddha medicine system and treatment of liver diseases. This article is focused to study on the structural, optical, morphological, and dielectric characteristics of both AgO NPs synthesized using a simple and green synthesis method. The antimicrobial activity of the present samples is also examined for biological applications.

2 Materials and methods

2.1 Chemicals and plant collection

The silver nitrate ($AgNO_3$, manufactured by Merck with a high purity of 99%) was used to synthesize AgO NPs using a green manufacturing process. *Solanum nigrum* (black nightshade) and *Mentha* (mint) are the well-known herbal plants cultivated in good loam and black soil in Peramandapatti village, Karimangalam Taluk, Dharmapuri district, Tamil Nadu, India. Naturally, the soil of the district is relatively soft and fresh, varying in color from red to deep brown. *Solanum nigrum* plants were harvested for their tender, greenish-yellow leaves, which were then cleaned under running water, twice or three times, and then with distilled water. Each leaf was meticulously washed using a white Khadhi cloth before being dried for 3 hours at room temperature.

2.2 Synthesis of AgO NPs

Normal water, distilled water, and acetone were used to clean all glassware. In a 100 mL beaker, 10 g of *Solanum nigrum* and *Mentha* leaves was boiled with 50 mL of distilled water at 80°C for 20 min. To remove the particulate matter and obtain clear solutions, the various leaf extracts were filtered through the Whatman No. 1 filter paper in a 250 mL beaker, and 50 mL of 0.5 M $AgNO_3$ was placed and stirred for 20 min. Then, at room temperature, 10 mL of plant extracts (*Solanum nigrum*, *Mentha*) was added separately to it. For 20 min, the solution was vigorously stirred. When the reaction is initiated, the color of the solution changes from light pale yellow to dark brown. The final AgO NP product was dried in a hot air oven for 2 h at 80°C. Dried samples were characterized to analyze the properties of the prepared nanomaterials [18–20]. The detailed flow chart of the synthesis method is given in Figure 1b.

As a multivalent element, silver interacts with oxygen to form a variety of phases, including Ag_2O, AgO, Ag_3O_4, and Ag_2O_3. These phases include AgO NPs, a fascinating class of metal oxides. Due to the absence of annealing in the synthesis of silver oxide, Ag and AgO are the most observable phases in experiments. It has also been revealed that they decompose at temperatures lower than 250°C [21].

2.3 Characterization of AgO NPs

XRD is the most commonly used technique for investigating chemical compounds as well as determining the crystal structure and size of AgO NPs using Cu-K1 radiation with a wavelength of 1.5406 Å. Scanning electron microscopy (SEM) is an electron microscopy technique that provides the speed and high resolution of a direct surface image while also measuring dimensions (size and shape) at micro- and nanoscales. Filed emission scanning electron microscope (FESEM) (Hitachi 6600, Tokyo) was used to examine the particle aggregation degree and purity. The morphology,

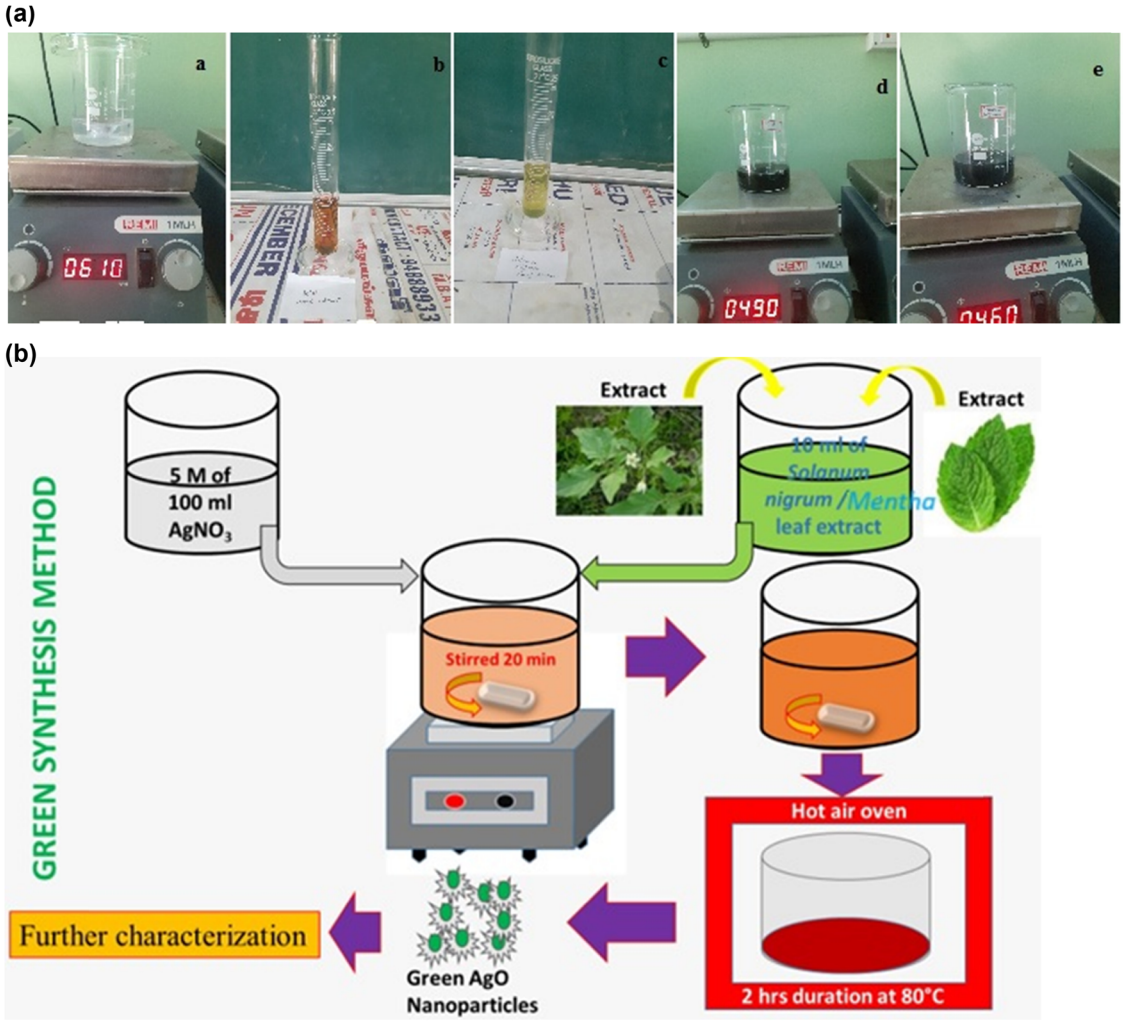

Figure 1: (a) AgO NP synthesis process: a (0.5 M)$AgNO_3$ solution, (b) and (c) 10 mL *Mentha* and *Solanum nigrum* leaf extracts; (d) and (e) show the synthesized AgONPs from *Mentha* and *Solanum nigrum* leaf extracts. (b) Schematic diagram of AgO NPs extract from *Solanum nigrum*/*Mentha* leaf by the green synthesis method.

size, and crystallinity of the AgO NPs were examined using high-resolution transmission electron microscopy (HRTEM, JEOL-JEM-2100 PLUS, Japan) and a selected area electron diffraction (SAED) pattern. Fourier transform infrared spectroscopy (FTIR) is a reliable, simple, and widely used analytical technique for screening and determining whether or not biological molecules of NPs are involved in the synthesis. FTIR spectral analysis was used to identify the biomolecules that acted as reducing and capping agents during the AgONP synthesis process. UV–visible (UV–vis) absorption spectroscopy (Shimadzu instrument in diffuse reflectance spectra (DRS) mode) is a valuable technique for characterizing the absorbance bands and band gaps of NPs, particularly those of noble metals. Energy dispersive X-ray spectroscopy is a spectroscopic technique used to determine the elemental composition and purity of AgO NPs that have been synthesized.

2.4 Antimicrobial activity of AgO NPs

The given samples were tested for antimicrobial activity by the well-diffusion method. Liquid Mueller Hinton agar media and the Petri plates were sterilized by autoclaving at 121°C for about 30 min at 15 lbs pressure. Under aseptic conditions in the laminar airflow chamber, about 20 mL of the agar medium was dispensed into each Petri plate to yield a uniform depth of 4 mm. After solidification of the media, 18 h culture of Gram-positive microorganisms, such as *Bacillus cereus (MTCC 430), Staphylococcus aureus (MTCC 3160)*, and Gram-negative microorganisms, such as *Escherichia coli (MTCC 1698)* and *Klebsiella pneumoniae (MTCC10309)*, obtained from IMTECH, Chandigarh, were swabbed on the surface of the agar plates. The well was prepared by using a cork borer followed by loading of 50

and 100 µL of each sample to the distinct well with sterile distilled water as negative control and tetracycline (30 mcg·disk^{-1}) as positive control. The sample-loaded plates were then incubated at 37°C for 24 h to observe the zone of inhibition.

3 Results

3.1 Crystal structure analysis

The powder XRD of AgO NPs is depicted in Figure 2. The XRD spectra of the synthesized NP revealed that the four main prominent diffraction peaks were observed at 2θ = 38.07, 44.24, 64.36, and 77.33 for *Mentha* and 38.06, 44.25, 64.35, and 77.32 for *Solanum nigrum*, which correspond to the (111), (200), (220), and (311) planes of silver and can be indexed as the cubic phase of Ag, and these results are well matching with JCPDS card No. 04-0783. The presence of strong peaks in the diffraction pattern confirms the high crystalline characteristics of the synthesized materials. There is a minor peak position at an angle of 27.76° (112), 32.17° (202), 46.17° (132), 54.74° (224), and 57.43° (402), 67.38° (206), and 76.71° (136) for *Mentha*. The same planes were seen in *Solanum nigrum*-mediated AgONPs, with a slight change in 2θ values of 27.68° (112), 32.18° (202), 46.16° (132), 54.79° (224), and 57.28° (402), respectively, for *Solanum nigrum*, which represents the presence of other phases in the synthesized AgO NPs because of the incorporation of leaf extract, which is well matched with the standard JCPDS data of AgO (JCPDS No. 84-1108). According to the low-intensity peaks for AgO, the synthesized Ag/AgO sample primarily contains Ag NPs with very little AgO present [21]. To determine the crystallite size of NPs, the Debye–Scherrer formula was applied and the results are shown in Table 1 [22,23].

$$D = \frac{k\lambda}{\beta \cos\theta} \tag{1}$$

where λ denotes the wavelength of X-ray in nm (Cu-Kα_1, λ = 1.5406 Å), β is the full-width-at-half-maximum of the highest peak intensity, θ is the Bragg angle in degree, k indicates the shape factor (k = 0.9), and the lattice constant (4.085 Å) is calculated by using the following expression [24,25]:

$$\frac{1}{d^2} = \frac{h^2 + k^2 + l^2}{a^2} \tag{2}$$

where *hkl* is the Miller index of the planes, d is the distance between the planes, and a is the lattice constant.

3.2 FTIR spectroscopy

The connection of the functional groups was examined by matching the FTIR spectra of AgO NPs from *Solanum nigrum* and *Mentha* leaf, as shown in Figure 3. The absorption peaks around 3,436 and 1,386 cm^{-1} correspond to COOH or OH groups. The peaks at the wave numbers 2,919 and 1,606 cm^{-1} are appropriate to the vibration of the C–H, C–C, and –C═C–stretching of covalent vibration bonds, respectively. The vibration absorption peak at 545 cm^{-1} is related to the Ag–O. Additionally, weak absorption peaks are observed in the spectra due to Ag ion bond [26,27].

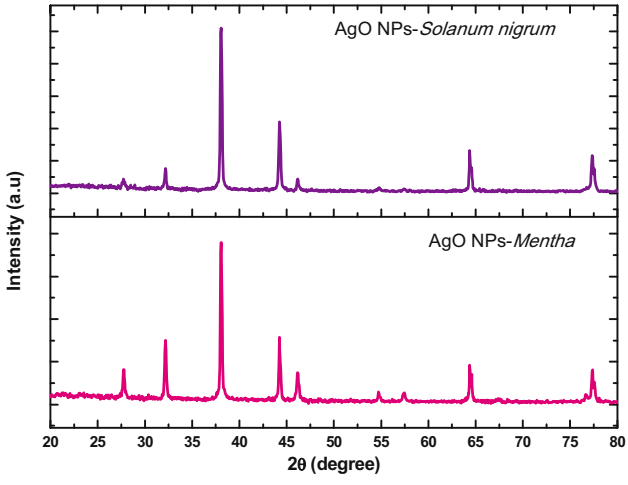

Figure 2: XRD spectra of AgO NPs from the extract of *Solanum nigrum* and *Mentha* leaf.

3.3 EDX spectra

Figure 4 shows the EDX spectra of the green synthesized AgO NPs. In addition to Ag and O, images display the Cl

Table 1: XRD raw data and average crystalline size of AgO NPs

2θ	Interplanar spacing (d) Å	FWHM (deg)	Crystallite size (D) 10^{-9}	Average crystallite size (D) 10^{-9}
38.104	2.363	0.197	36.942	28.71
44.194	2.047	0.197	31.850	
64.366	1.447	0.197	21.862	
77.429	1.234	0.148	24.199	

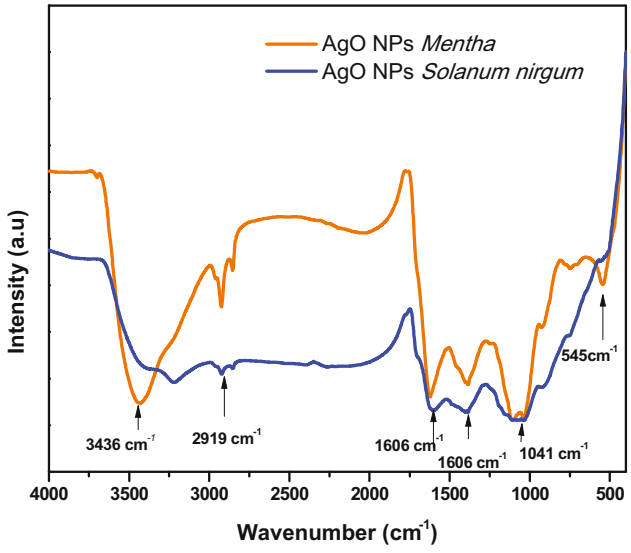

Figure 3: FTIR spectra of AgO NPs from the extract of *Solanum nigrum* and *Mentha* leaf.

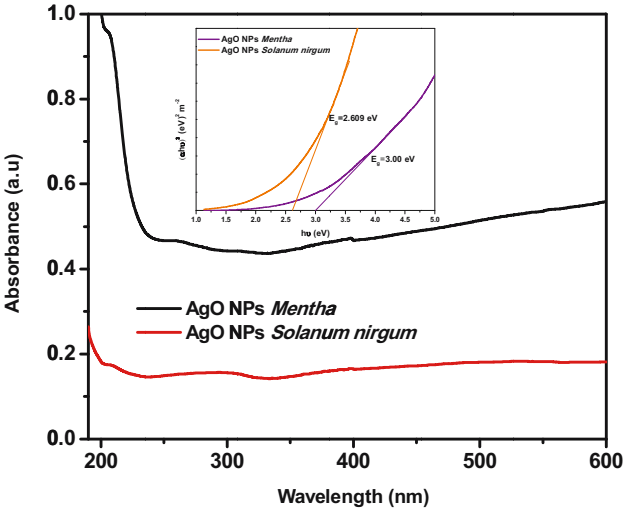

Figure 5: Optical absorbance spectra of AgO NPs from the extract of *Solanum nigrum* and *Mentha* leaves.

peaks that originated from the synthesis route [28]. The corresponding weight and atomic percentage were also calculated, and the variation was observed in both samples [29]. The results showed that *Solanum nigrum* has a high weight and atomic percentage.

3.4 UV–vis absorbance spectroscopy

The optical property of a metal NP was investigated using UV–vis DRS analysis. Although the peak was missing, the absorbance band edge of AgO NPs was observed around 397.55 nm (*Mentha*) and 293.50 nm (*Solanum nigrum*), respectively [30]. Interestingly, the *Solanum nigrum* AgO NPs have very low absorbance when it is compared with *Mentha* AgO NPs. The expression for the Kubelka–Munk function is as follows:

$$\alpha = \frac{4\pi k}{\lambda} \tag{3}$$

The optical band gap energy can be calculated by using the following equation [31].

$$(\alpha h\nu)^n = C(h\nu - E_g) \tag{4}$$

where $h\nu$ is the incident photon energy, C is the proportionality constant, E_g is the band gap (eV), and n is the power factor representing allowed indirect and direct transitions for the n values of 0.5 and 2, respectively. The quantity $[\alpha h\nu]^2$ is plotted as a function of the incident photon

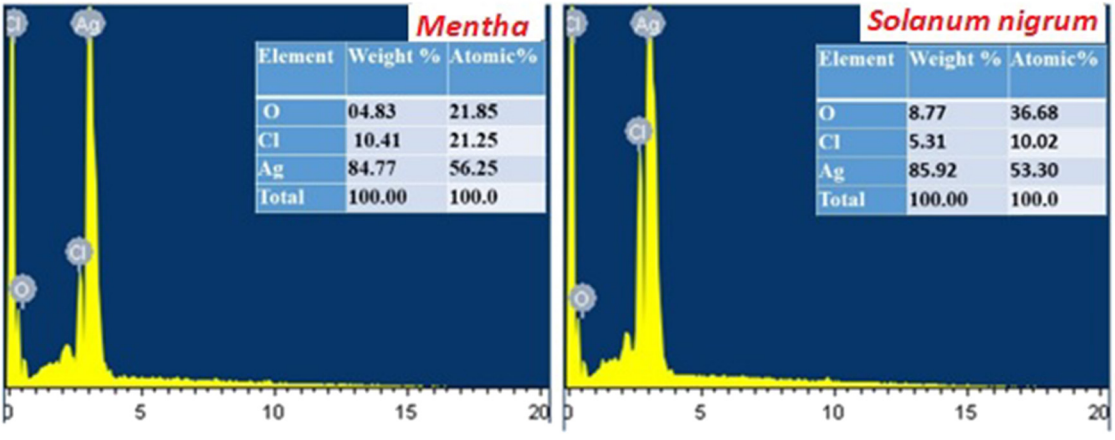

Figure 4: EDX images of AgO sample display the presence of Ag, oxygen, and chlorine (less percentage) in AgO NPs measured from EDX spectroscopy.

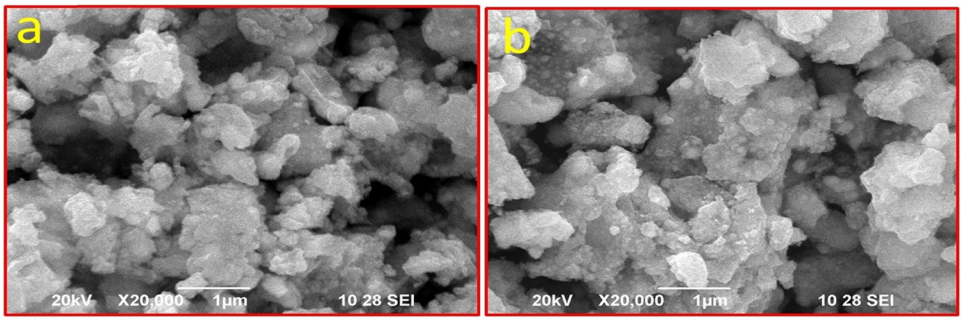

Figure 6: FESEM image for AgO NPs from the extract of (a) *Solanum nigrum* and (b) *Mentha* leaf.

energy *hv* to determine the optical band gap E_g from the point of interception with the *X*-axis. Band gap energy (E_g) of AgO NPs is calculated, using the Kubelka–Munk relationship [31], and the obtained band gap energy values are found to be 2.609 and 3.00 eV for *Solanum nigrum* and *Mentha* leaf extract, respectively (Figure 5).

3.5 Surface morphological studies

Figure 6(a) and (b) shows the FESEM image of 1 μm magnification for AgO NP synthesis from the extract of *Solanum nigrum* and *Mentha* leaves. It seems that AgO NPs from *Solanum nigrum* leaf extract have different kinds of

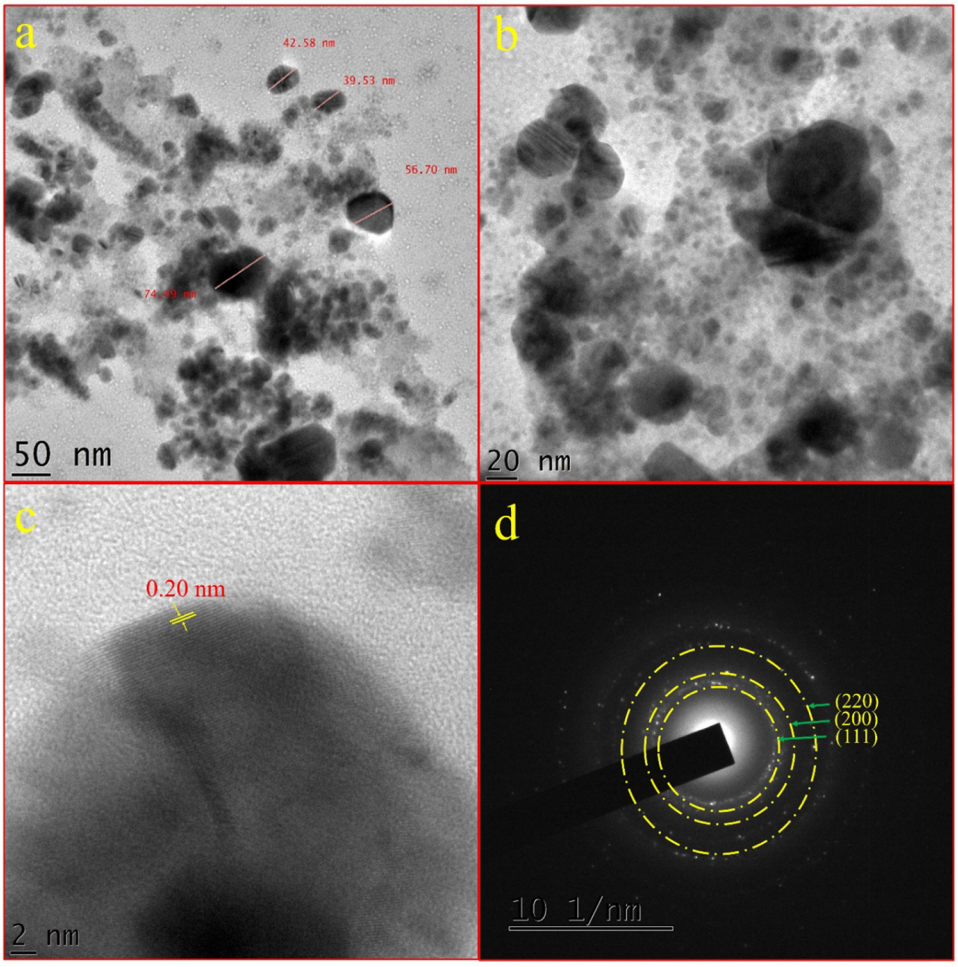

Figure 7: TEM image for AgO NPs synthesized by *Solanum nigrum* leaf extract at different scale bars. (a: 50 nm; b: 20 nm; c: 2 nm; d: 1 nm), respectively.

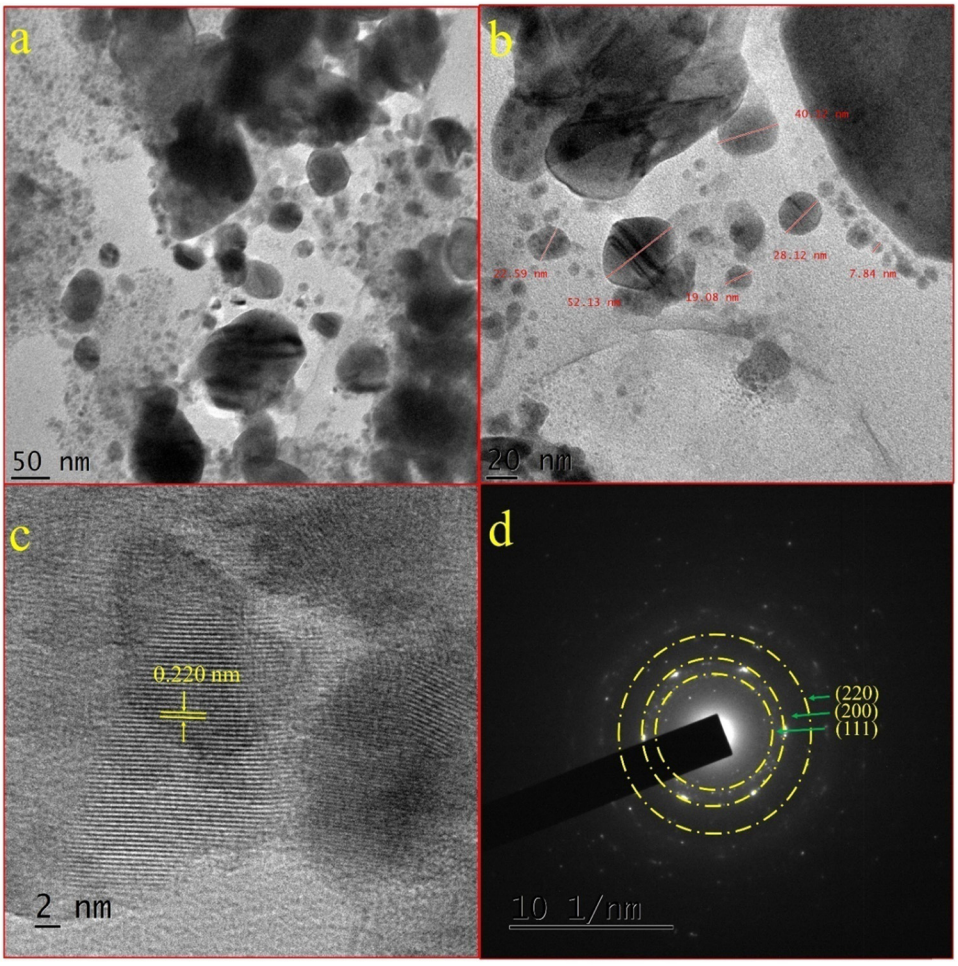

Figure 8: TEM image for AgO NPs synthesized by *Mentha leaf* extract at different scale bars. (a: 50 nm; b: 20 nm; c: 2 nm; d: 1 nm), respectively.

structures such as a flower and small spherical ball shapes on top of the flower with more voids. However, AgO NPs from *Mentha* leaf extract show a similar kind of flower structure with minimal voids. The result of minimal voids in the sample gives better antibacterial activity than other species [32,33].

The structural morphology and particle size of AgO NPs were examined by transmission electron microscopy (TEM). Figures 7 and 8 display different magnifications of TEM bright field images, HRTEM, and SAED patterns for AgO NPs. Sample preparation for TEM analysis consists of AgO NPs from leaf extract dispersed in 1 mL of ethanol and sonicated for half an hour to obtain a well-mixed solution. The mixed solution was dropped on a copper grid and then dried at 60°C in an open-air atmosphere. The results revealed the clouds of spherical ball structures in different scale sizes. The AgO NPs indicate a size of 7–56 nm with an average size of 30 nm. Figures 7(c) and (d) and 8(c) and (d) display the interplanar spacing (fringe width) values of 0.20 and 0.220 nm of *Solanum nigrum* and *Mentha* AgO NP samples, which clearly indicates the lattice spacing of plane (200) and (111), respectively. The results are well coordinated with XRD results.

3.6 Determination of antimicrobial activity by agar well diffusion method (AWDM)

The antibacterial activities of the synthesized AgO NPs were observed against Gram-positive (*Staphylococcus aureus*, *Bacillus cereus*) and Gram-negative bacteria (*Klebsiella pneumonia*, *Escherichia coli*) by AWDM. The various sizes (in mm) of the zone of inhibition results were compared with two different leaf extracts. Antibacterial activities of the green synthesized AgO NPs solution from *Solanum nigrum* leaf extract were tested against *Mentha* leaf, which was studied using bacteria such as *Staphylococcus aureus*,

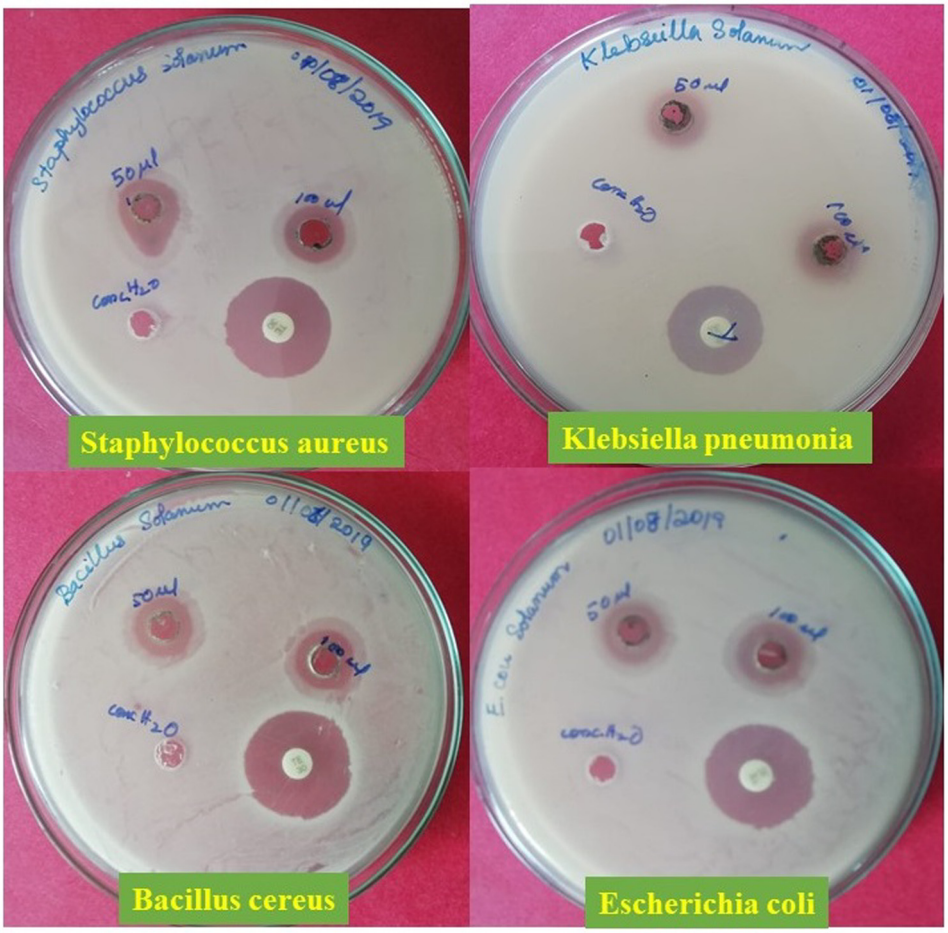

Figure 9: Antimicrobial activity of AgO NPs synthesized by *Solanum nigrum* leaf extract.

Bacillus cereus, *Escherichia coli*, and *Klebsiella pneumonia*. In this, 0.4 molar concentration of AgO NP solution was used, since one molar of AgO NPs gives a vast-prevent diameter region, leading to an overlap in the regions. As a result, the microbial halo formed around the NP solution, which indicates that the green synthesized AgO NPs have excellent antimicrobial activity [34,35]. Particularly, the AgO NPs from *Mentha* leaves show an excellent antimicrobial prevention activity compared to *Solanum nigrum* leaf extract as shown in Figures 9 and 10 and Table 2. The AgO NPs react with the bacteria cell region and prevent the respiratory process by interacting with AgO NPs with the respiratory enzymes. As shown in Figures 9 and 10, Gram-positive (*Staphylococcus aureus*) and Gram-negative bacteria (*Escherichia coli*) show large prevention area diameters. In difference, Gram-positive (*Bacillus cereus*) and Gram-negative (Klebsiella *pneumonia*) bacteria show a lower prevention diameter as shown in Figures 9 and 10. The difference in the constrained diameter is assigned to the range of the bacteria cell zone [36]. Thus, the basic principle of antibacterial activity in this study is ascribed to the high surface area-to-volume ratio between AgO NPs and bacteria.

3.7 Electrical analysis

The dielectric analysis is a useful tool for understanding the grain boundaries, the microstructure of the compound, its transport properties, charge-storage capacity, etc [37]. At different temperatures, the dielectric properties, such as capacitance and the loss factor (or dissipation factor) of AgO NPs derived from leaf extract of *Solanum nigrum*/*Mentha*, were measured in the frequency range of 4 Hz to 8 MHz. Figure 11(a and b) illustrates the dielectric permittivity (ε_r) and dielectric loss for both AgO NPs as a function of frequency at various temperatures. The value of ε_r decreases fast as frequency increases and approaches a constant limiting point at which ε_r essentially becomes frequency dependent, which is attributed to the reduction

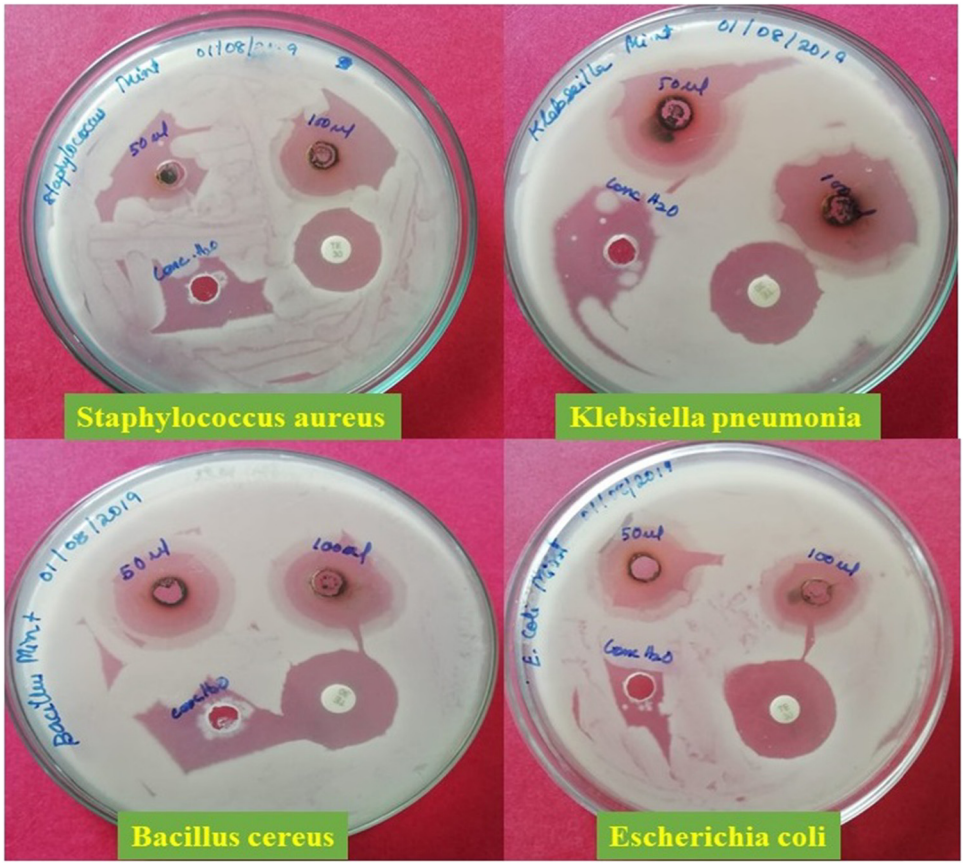

Figure 10: Antimicrobial activity of AgO NPs from *Mentha* leaf extract.

of domain walls, as can be seen from the frequency-dependent plot of ε_r. In this case, the dipoles can simply align in the applied field direction. As a result of the dominance of space charge polarization in both samples, the dielectric constant of all samples has a greater value at low frequencies and practically reaches a constant value after 1 kHz. This distinctive behavior of polar dielectrics may be understood using the Koop and Maxwell Wagner theory, which makes the assumption that the dielectric medium is composed of conducting grains separated by relatively resistive grain boundaries [38,39]. The nanocrystal sizes of the generated samples are another factor in the behavior of the samples. Dislocations, defects, and voids create declination in the dielectric constant at the nanoscale, which results in constant values of ε_r [40].

Figure 11(b) displays the variations in dielectric loss with frequency for both AgO NPs. The change in tan δ reached the constant value up to 10 kHz, and then the loss factor increases with increasing frequency. The synthesis process can have an impact on the behavior of leaf

Table 2: Maximum zone of inhibition by AgO NPs synthesized by *Solanum nigrum* and *Mentha* leaf extract

S. no.	Microorganisms	Zone of inhibition in diameter (mm)					
		Control (100 µg·mL^{-1})	*Mentha*		*Solanum nigrum*		Std. antibiotic (tetracycline) 30 mcg·disk^{-1}
			50 µg·mL^{-1}	100 µg·mL^{-1}	50 µg·mL^{-1}	100 µg·mL^{-1}	
1	*Bacillus cereus*	Nil	10	12	7	12	24
2	*Staphylococcus aureus*	Nil	14	20	6	8	26
3	*Escherichia coli*	Nil	10	15	8	9	25
4	*Klebsiella pneumoniae*	Nil	16	18	10	18	25

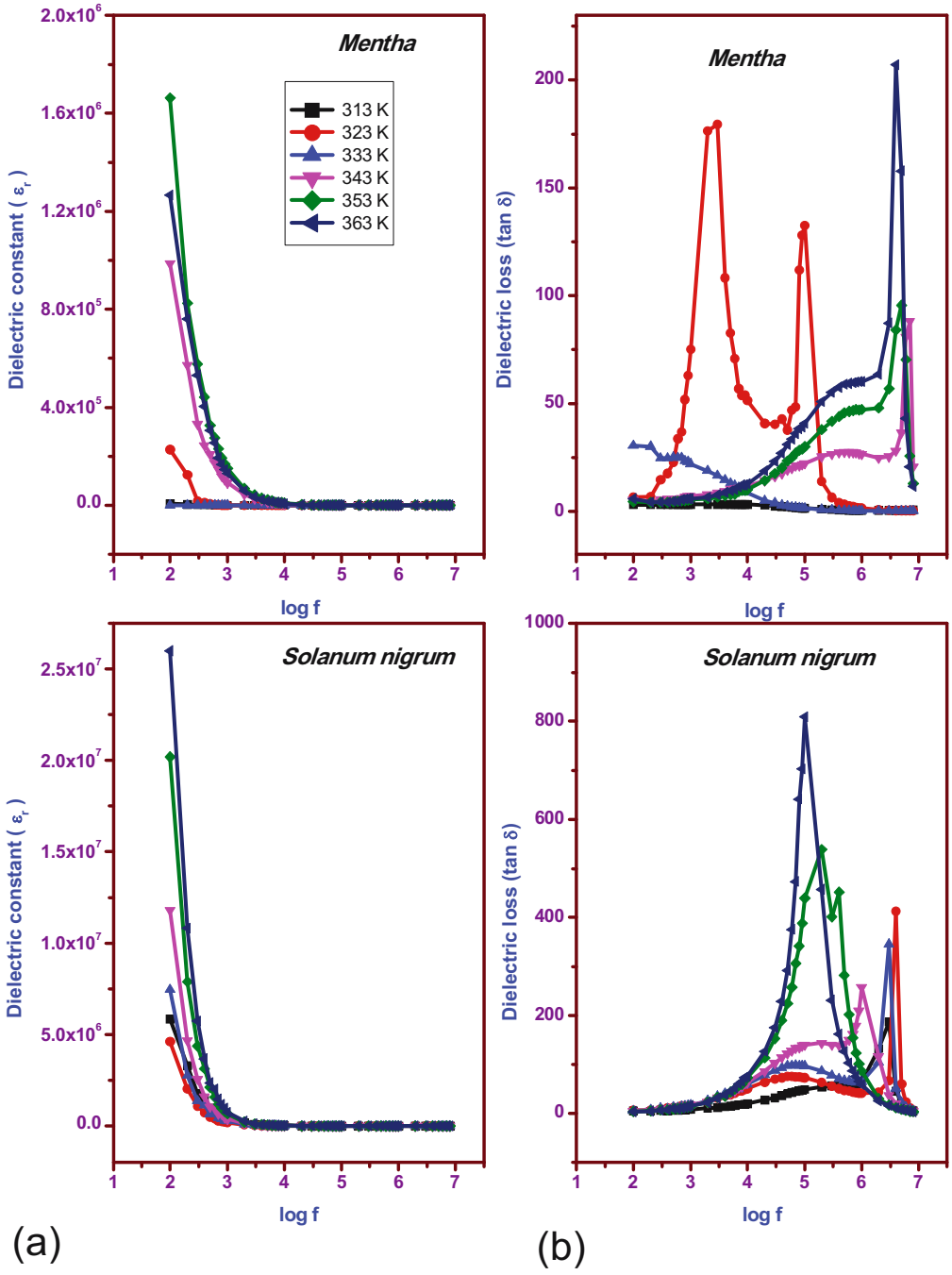

Figure 11: Illustrating *Solanum nigrum/Mentha* of leaf extract AgO NPs for 313, 323, 333, 343, and 353 K (various frequencies): (a) dielectric constant and (b) dielectric loss.

extract, sample homogeneity, structural stoichiometry, and other factors that might cause changes in dielectric loss [41].

Figure 12(a and b) indicates that both AgO NPs exhibit the greatest value of dielectric constant and δ, whereas the AgO NPs of *Solanum nigrum* leaf extract exhibit high values compared with the AgO NPs of *Mentha* leaf extract. Their resistance may play a part in the cause [42]. Therefore, the energy loss of both AgO NPs cannot be influenced by Ag^{+} ions. Previous studies have reported similar behaviors of ε_r and tanδ for these samples. The tan δ curves of both samples showed some additional peaks. Particularly, the AgO NPs of *Solanum nigrum* leaf extract at 323 K explore the two peaks, which may be due to lack of resistance.

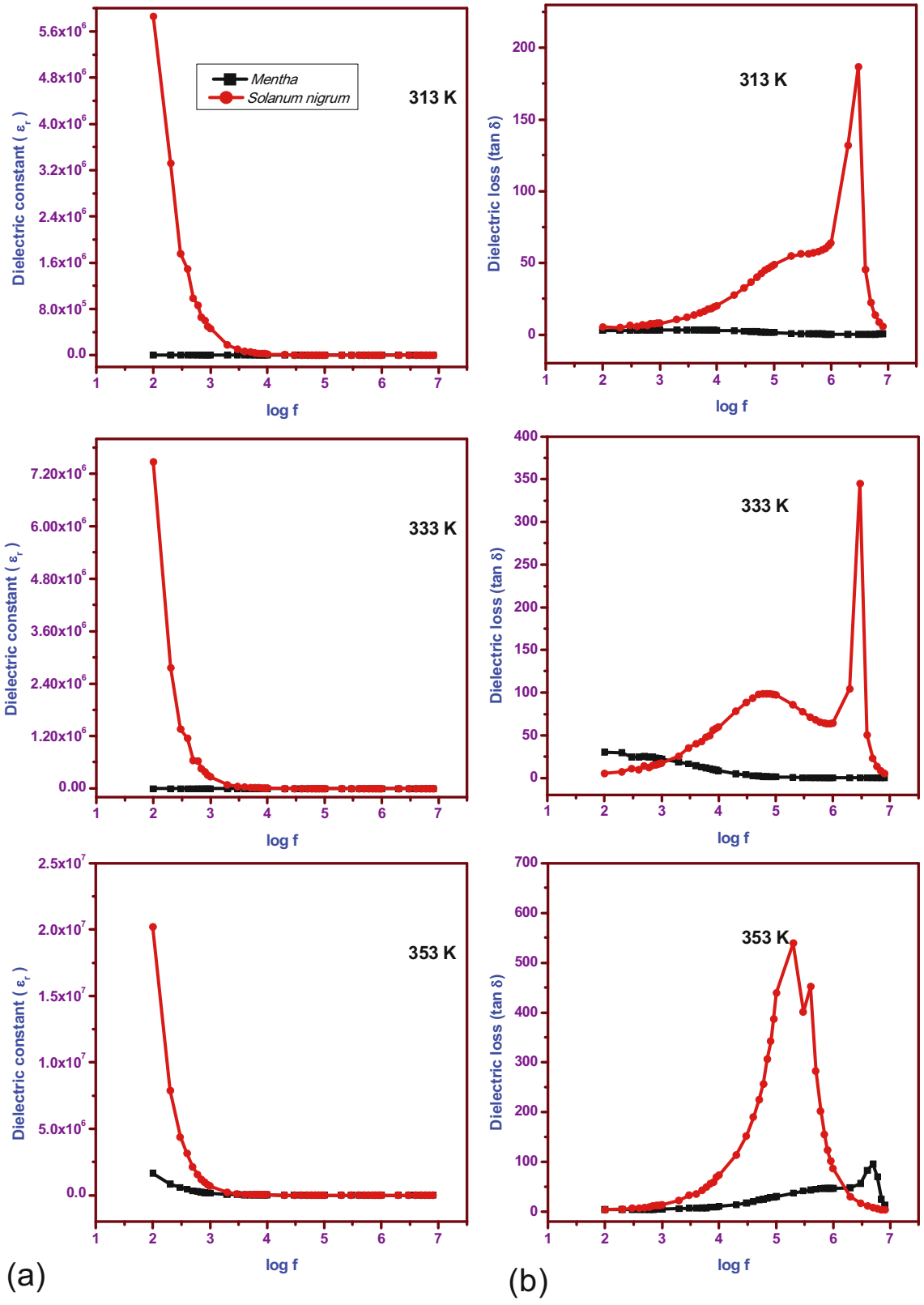

Figure 12: Difference of *Solanum nigrum* and *Mentha* of leaf extract AgO NPs for 313, 333, and 353 K (various frequencies): (a) dielectric constant and (b) dielectric loss.

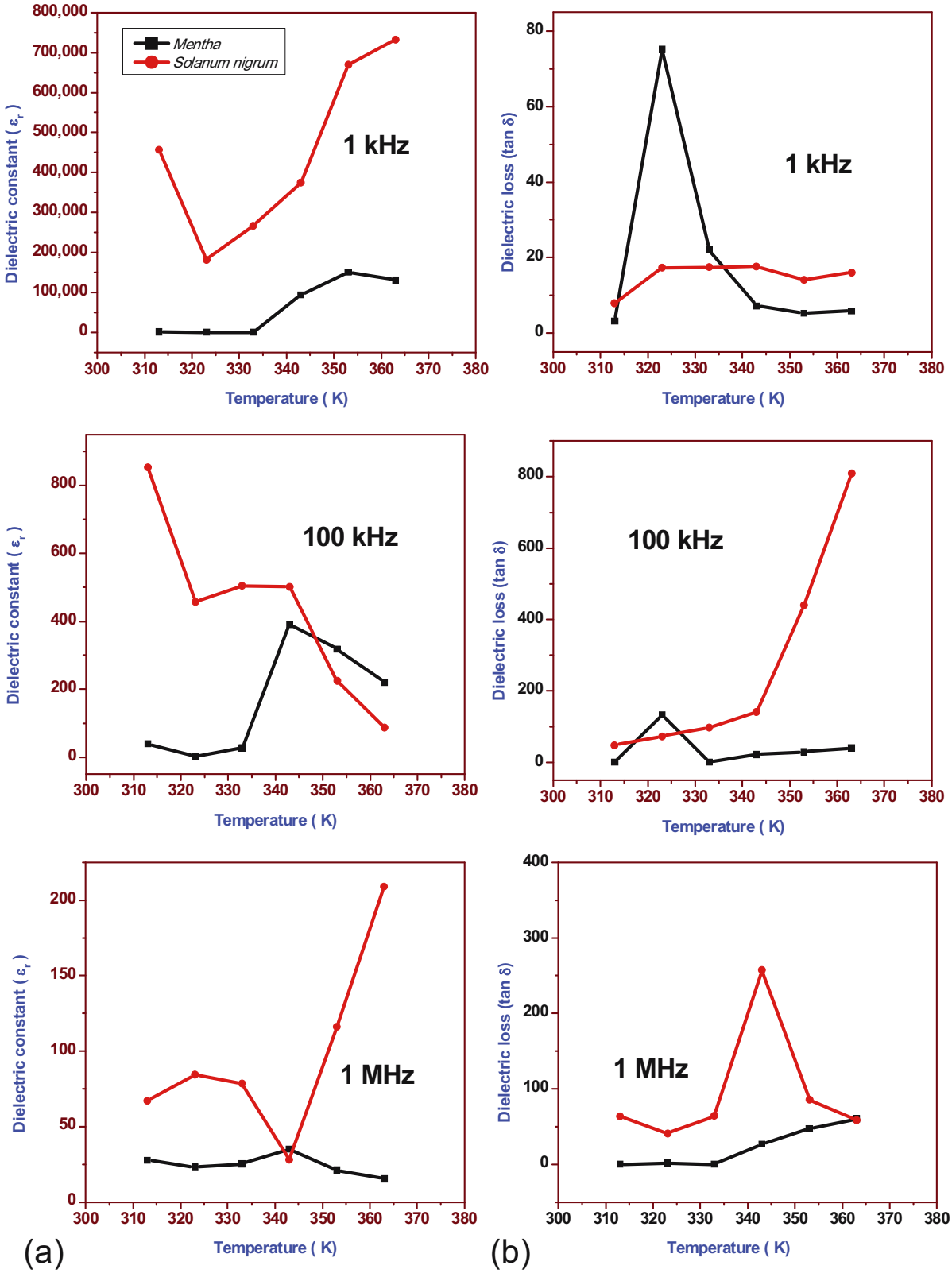

Figure 13: Difference of *Solanum nigrum* and *Mentha* of leaf extract AgO NPs for 1 kHz, 100 kHz, and 1 MHz (temperature dependence): (a) dielectric constant and (b) dielectric loss.

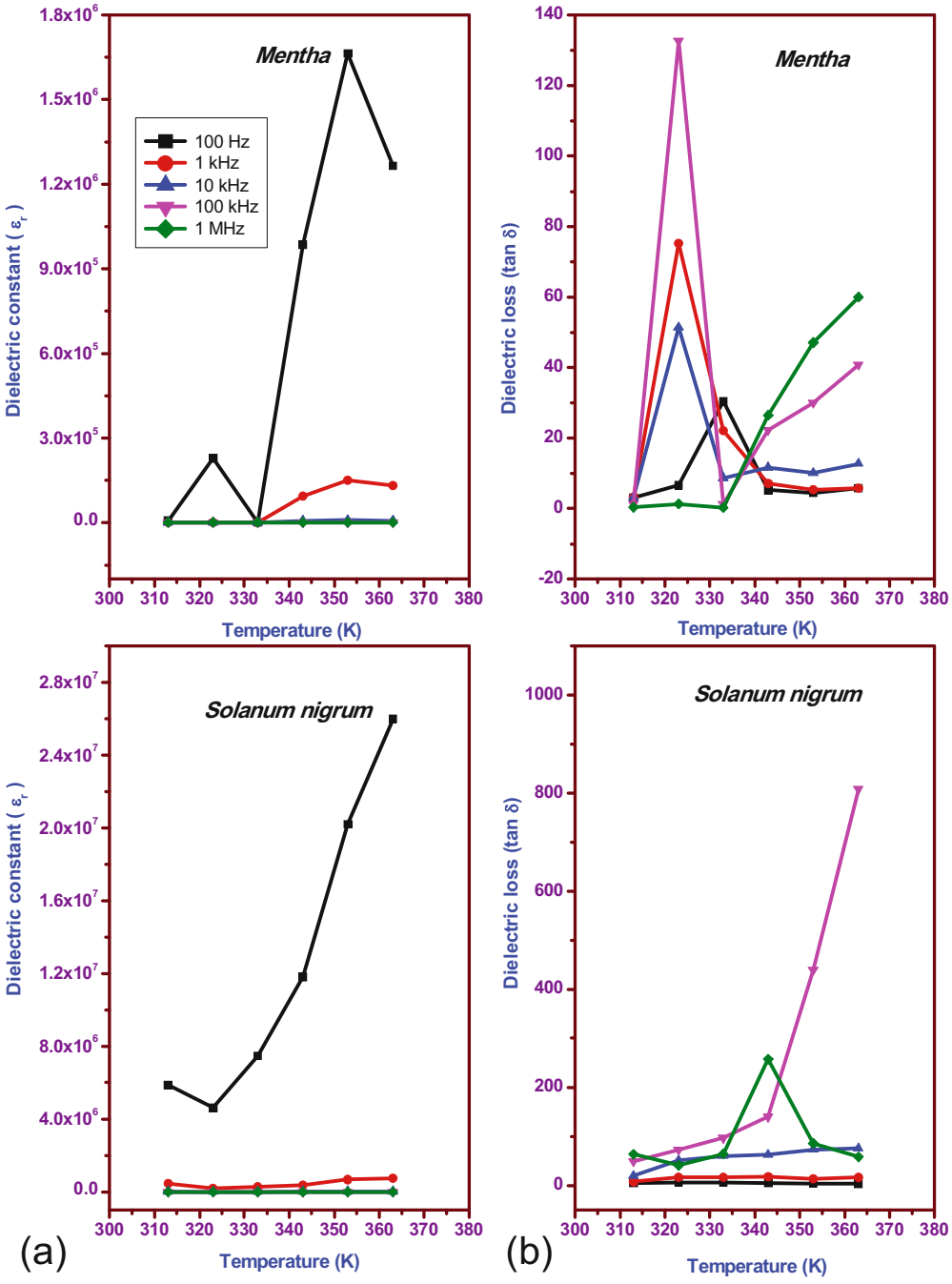

Figure 14: *Solanum nigrum*/*Mentha* leaf extract AgO NPs for 100 Hz, 1 kHz, 10 kHz, 100 kHz, and 1 MHz (temperature dependence): (a) dielectric constant and (b) dielectric loss.

In order to distinguish between the effects of intrinsic dielectric polarization and space charge polarization, the ε_r and tan δ were plotted as a function of temperature at chosen frequencies of 1 kHz, 100 kHz, and 1 MHz, which are shown in Figure 13(a and b). Figure 13(a) shows that at all specified frequencies, the values of the dielectric constants rise with rising temperature. The dielectric constant changes with temperature at different frequencies as shown by the following. Since the thermal energy at low temperatures is insufficient to liberate the localized electric dipoles, the dielectric constant initially rises a little with increasing temperature. These dipoles make an effort to realign themselves toward the electric field being delivered outside. The direction of the dipoles in the presence of an external electric field determines the dipole polarization [43,44]. The arrangement of the dipoles gets more

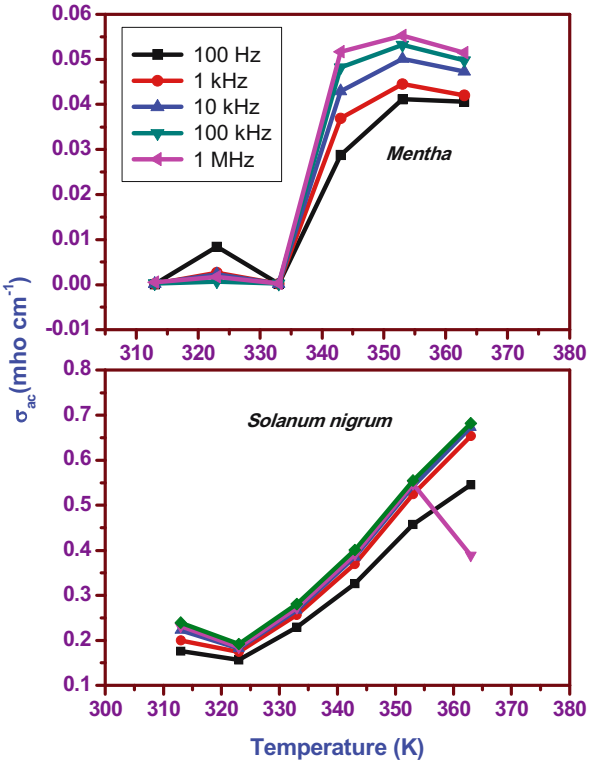

Figure 15: Variation of AC electrical conductivities with temperatures at different frequencies for *Solanum nigrum*/*Mentha* of leaf extract AgO NPs.

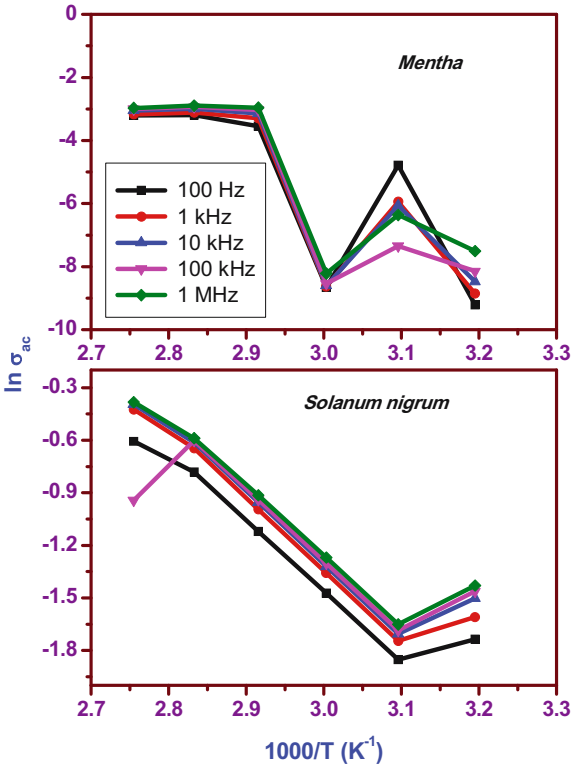

Figure 16: Plot of ln(σ_{ac}) T versus 1,000/T for *Solanum nigrum/Mentha* of leaf extract AgO NPs.

challenging as the temperature rises due to an increase in entropy, which causes the dipole polarization to decrease as the temperature rises.

Figure 14(a and b) makes it very evident that the AgO NPs of *Solanum nigrum* leaf extract are high when compared to the AgO NPs of *Mentha* leaf extract and both the dielectric constant and dielectric loss rise. The study made on solids to characterize the resistance of the crystalline sample is AC conductivity, another significant attribute of the sample. The AC conductivity may be measured using a variety of techniques depending on the dielectric data [45,46]. In Figure 15, the variation in AC electrical conductivity is shown as a function of temperatures for both AgO NPs and their embedding with various leaf extracts at different frequencies. The conductivity spectrum exhibits a unique conductivity dispersion in the frequency range of 100 Hz, 1 kHz, 10 kHz, 100 kHz, and 1 MHz. This graph shows the relationship between conductivity and frequency. As frequency decreases, there is an increasing charge accumulation at the electrode–sample contact, which causes this to happen. As a result, there are fewer mobile ions present, which reduces the conductivity at low frequencies. The conductivity of materials increases as frequency increases because charge carriers are more mobile at higher frequencies [47]. Figure 16 depicts the ln σ_{ac} versus 1/T graph, which follows the Arrhenius

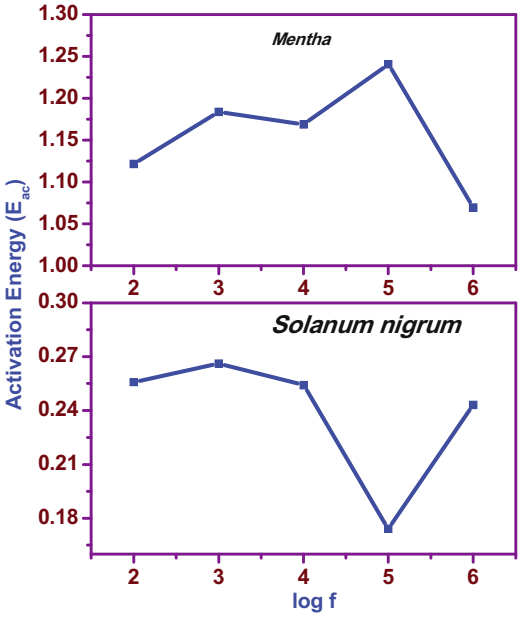

Figure 17: Variation of AC activation energy with log frequency for *Solanum nigrum/Mentha* of leaf extract AgO NPs.

relationship. Electrical conductivity was improved by adding extract. The impurities in the material have an impact on the

activation energy decrease for the AgO NPs of *Solanum nigrum* leaf extract and increase for AgO NPs of *Mentha* leaf extract, which is illustrated in Figure 17. A little portion of the activation energy produced from the AC conductance calculation is useful for the production of electro-optical devices.

4 Conclusions

Green synthesis of AgO NPs using biological agents is of ecologically low cost and capable of producing NPs at room temperature. The cubic structure of the synthesis product was confirmed by XRD results with an average particle size of 28.71 nm. From a Touc plot, the optical band gap of the products is found to be 2.609 and 3.00 eV for *Solanum nigrum* and *Mentha* leaf extract, respectively. The FTIR spectra show the existence of a functional group, absorbance peaks at 3,436, 2,919, 1,606, 1,386, 1,041, and 545 cm^{-1} corresponding to –OH, $–CH_2$, –COOH, C–C, C–C, C–H, and Ag–O groups, respectively. The SEM and TEM results show that the structural morphology of AgO NPs, which consists of varied shapes such as flower kind of structure with a small spherical on top of the flower surface, gives more bacterial activity. AgO NPs prepared from *Solanum nigrum* leaf extract and their dielectric dispersion behavior demonstrate that thermal hopping of space charges occurs in all of the samples. In contrast, the AgO NPs of *Solanum nigrum* leaf extract show higher values when compared to the AgO NPs of *Mentha* leaf extract. The examination of the dielectric reveals that at high frequencies, both dielectric dispersion components diminish, preventing interface dipoles from swiftly traveling to the alternate zone. A low dielectric dispersion is frequently preferred for a variety of applications, including high-speed integrated packages and satellite communication applications. Furthermore, the conductivity of both samples remains virtually constant up to a certain frequency, before rapidly rising. As a result, it has been demonstrated that the material is a good candidate for optoelectronic applications. In addition, the silver NPs synthesized using *Mentha* leaf extract exhibited better antibacterial activity than *Solanum nigrum*. This may be used as a potential candidate for antibacterial microbes.

Acknowledgements: The authors are thankful to the Deanship of Scientific Research at the University of Bisha, Saudi Arabia. This work was supported by the Fast-Track Research Support Program.

Funding information: Authors state no funding involved.

Author contributions: Conceptualization and methodology – Subramanian Mohanaparameswari and Manavalan Balachandramohan; formal analysis – Ponnusamy Sasikumar and Mark Vimalan; investigation and data curation – Salim Albukhaty and Ghassan M. Sulaiman; validation – Mosleh M. Abomughaid and Mohammed Abu-Alghayth; visualization – Mosleh M. Abomughaid; original draft preparation– Krishnamurthy Ganesh Kumar, Chinnaiyan Rajeevgandhi, Sanmugam Pugazhendhi, and Manavalan Balachandramohan; supervision – Manavalan Balachandramohan, Mark Vimalan, Salim Albukhaty, and Ponnusamy Sasikumar; project administration – Manavalan Balachandramohan and Ponnusamy Sasikumar. All authors gave approval to the final version of this manuscript.

Conflict of interest: The authors state no conflict of interest.

Data availability statement: The datasets generated during and/or analysed during the current study are available from the corresponding author on reasonable request.

References

[1] Alhujaily M, Albukhaty S, Yusuf M, Mohammed MKA, Sulaiman GM, Al-KarAgly H, et al. Recent advances in plant-mediated zinc oxide nanoparticles with their significant biomedical properties. Bioengineering. 2022;9(10):541 (19 Pages). doi: 10.3390/bioengineering9100541.

[2] Al-Karagoly H, Rhyaf A, Naji H, Albukhaty S, AlMalki FA, Alyamani AA, et al. Green synthesis, characterization, cytotoxicity, and antimicrobial activity of iron oxide nanoparticles using Nigella sativa seed extract. Green Process Synth. 2022;11(1):254–65. doi: 10.1515/gps-2022-0026.

[3] Muthukrishnan S, Bhakya S, Kumar TS, Rao MV. Biosynthesis, characterization and antibacterial effect of plant-mediated silver nanoparticles using Ceropegia thwaitesii–An endemic species. Ind Crop Prod. 2015;63:119–24. doi: 10.1016/j.indcrop.2014.10.022.

[4] Bhakya S, Muthukrishnan S, Sukumaran M, Muthukumar M. Biogenic synthesis of silver nanoparticles and their antioxidant and antibacterial activity. Appl Nanosci. 2016;6:755–66. doi: 10.1007/s13204-015-0473-z.

[5] Mahmood RI, Kadhim AA, Ibraheem S, Albukhaty S, Mohammed-Salih HS, Abbas RH, et al. Biosynthesis of copper oxide nanoparticles mediated Annona muricata as cytotoxic and apoptosis inducer factor in breast cancer cell lines. Sci Rep. 2022;12:16165. doi: 10.1038/s41598-022-20360-y.

[6] Bhakya S, Selvaraj M, Sukumaran M, Muthukumar M, Senthil Kumar T, Rao M. Catalytic degradation of organic dyes using synthesized silver nanoparticles: A green approach. J Bioremediat Biodegrad. 2015;6:312. doi: 10.4172/2155-6199.1000312.

[7] Prabaharan N, Palanisamy K. A comprehensive review on reduced switch multilevel inverter topologies, modulation techniques and

applications. Renew Sustain Energy Rev. 2017;76:1248–82. doi: 10.1016/j.rser.2017.03.121.
[8] Saleh HM, Hassan AI. Synthesis and characterization of nanomaterials for application in cost-effective electrochemical devices. Sustainability. 2023;15(14):10891.
[9] Alzubaidi AK, Al-Kaabi WJ, Ali AA, Albukhaty S, Al-KarAgly H, Sulaiman GM, et al. Green synthesis and characterization of silver nanoparticles using *Flaxseed* extract and evaluation of their antibacterial and antioxidant activities. Appl Sci. 2023;13:2182. doi: 10.3390/app13042182.
[10] Khane Y, Benouis K, Albukhaty S, Sulaiman GM, Abomughaid MM, Al Ali A, et al. Green Synthesis of Silver Nanoparticles Using Aqueous *Citrus limon* Zest Extract: Characterization and Evaluation of Their Antioxidant and Antimicrobial Properties. Nanomaterials. 2022;12:2013. doi: 10.3390/nano12122013.
[11] Ashraf A, Zafar S, Zahid K, Salahuddin Shah M, Al-Ghanim KA, Al-Misned F, et al. Synthesis, characterization, and antibacterial potential of silver nanoparticles synthesized from *Coriandrum sativum* L. J Infect Public Health. 2019;12:275–81.
[12] El-Chaghaby GA, Ahmad AF. Biosynthesis of silver nanoparticles using *pistacia lentiscus* leaves extract and investigation of their antimicrobial effect. Orient J Chem. 2011;27:e929–36.
[13] Balasubramanian S, Jeyapaul U, Kala SMJ. Antibacterial activity of silver nanoparticles using Jasminum auriculatum stem extract. Int J Nanosci. 2019;18(01):1850011.
[14] Karthikeyan S, Selvapandiyan M, Sasikumar P, Parthibavaraman M, Nithiyanantham S, Srisuvetha VT. Investigation on the properties of vanadium doping WO_3 nanostructures by hydrothermal method. Mater Sci Energy Technol. 2022;5:411–5.
[15] Ahmed S, Ahmad M, Swami BL, Ikram S. Green synthesis of silver nanoparticles using Azadirachta indica aqueous leaf extract. J Radiat Res Appl Sci. 2016;9(1):1–7.
[16] Sasikumar P, Revathy MS, Nithiyanantham S. $Cd(OH)_2$ and CdO: structural, optical, electron density distribution analysis with antibacterial assay. Eur Phys J Plus. 2022;137(3):294.
[17] Shenbagavalli S, Muthuvinayagam M, Revathy MS, Sasikumar P. Ionic conductivity and dielectric studies on PVP/PEO/(NH_4) 2Ce $(NO_3)_6$ based solid polymer-blend electrolytes. Bull Mater Sci. 2022;45(3):125.
[18] Roy P, Das B, Mohanty A, Mohapatra S. Green synthesis of silver nanoparticles using Azadirachta indica leaf extract and its antimicrobial study. Appl Nanosci. 2017;7(8):843–50.
[19] Nagaraj G, Mohammed MK, Abdulzahraa HG, Sasikumar P, Karthikeyan S, Tamilarasu S. Effects of the surface of solar-light photocatalytic activity of Ag-doped TiO_2 nanohybrid material prepared with a novel approach. Appl Phys A. 2021;127:1–7.
[20] Manik UP, Nande A, Raut S, Dhoble SJ. Green synthesis of silver nanoparticles using plant leaf extraction of Artocarpus heterophylus and Azadirachta indica. Results Mater. 2020;6:100086.
[21] Dhoondia ZH, Chakraborty H. Lactobacillus mediated synthesis of silver oxide nanoparticles. Nanomater Nanotechnol. 2012;2:15.
[22] Kumar KG, Bhargav PB, Kumar GG, Aravinth K, Ahmed N, Balaji C. Structural and luminescence property evaluation of Sm3+ activated orange light emitting $Li_7La_3Zr_2O_{12}$ phosphors. Inorg Chem Commun. 2022;146:110188.
[23] Kumar KG, Bhargav PB, Aravinth K, Arumugam R, Ramasamy P, Pathi P. Reddish-orange-emitting $Ca_{12}Al_{14}O_{33}$:Sm^{3+} phosphors with high color purity. Chem Pap. 2022;76:1147–55.
[24] Mohammed MK, Al-Mousoi AK, Singh S, Kumar A, Hossain MK, Salih S, et al. Improving the performance of perovskite solar cells with carbon nanotubes as a hole transport layer. Optical Mater. 2023;138:113702.
[25] Nadeem M, Abbasi BH, Younas M, Ahmad W, Khan T. A review of the green syntheses and anti-microbial applications of gold nanoparticles. Green Chem Lett Rev. 2017;10(4):216–27.
[26] Sharma SN, Srivastava R. Silver oxide nanoparticles synthesized by green method from Artocarpus Hetrophyllus for antibacterial and antimicrobial applications. Mater Today Proc. 2020;28:332–6.
[27] Flores-Lopez NS, Cervantes-Chávez JA, Téllez de Jesús DG, Cortez-Valadez M, Estévez-González M, Esparza R. Bactericidal and fungicidal capacity of Ag_2O/Ag nanoparticles synthesized with Aloe vera extract. J Environ Sci Health Part A. 2021;56(7):762–8.
[28] Fayyadh AA, Jaduaa Alzubaidy MH. Green-synthesis of Ag_2O nanoparticles for antimicrobial assays. J Mech Behav Mater. 2021;30(1):228–36.
[29] Ganesh Kumar K, Balaji Bhargav P, Ahmed N, Balaji C. Influence of Sn doping on the structural, morphological, optical and photocatalytic functionality of ZnO nanostructures. Trans Electr Electron Mater. 2021;22:717–24.
[30] Saravanakumar K, Muthuraj V, Vadivel S. Constructing novel Ag nanoparticles anchored on MnO2 nanowires as an efficient visible light driven photocatalyst. RSC Adv. 2016;6(66):61357–66.
[31] Ganesh Kumar K, Balaji Bhargav P, Balaji C, Nafis A, Aravinth K, Ramasamy P. Effect of sintering on structural modification and phase transition of Al-substituted LLZO electrolytes for solid state battery applications. J Electrochem Energy Convers Storage. 2021;18(3):031012.
[32] Singh J, Dutta T, Kim KH, Rawat M, Samddar P, Kumar P. 'Green' synthesis of metals and their oxide nanoparticles: applications for environmental remediation. J Nanobiotechnol. 2018;16(1):1–24.
[33] Mehtab T, Yasin G, Arif M, Shakeel M, Korai RM, Nadeem M, et al. Metal-organic frameworks for energy storage devices: batteries and supercapacitors. J Energy Storage. 2019;21:632–46.
[34] Karthikeyan S, Srisuvetha VT, Vadivel S, Sathya P, Massou EES, Reddy VRM, et al. Study on preparation and performance of electrochemical supercapacitor based on La_2O_3/CNTs composites for energy storage applications. Chem Phys. 2023;568:111849.
[35] Singh JA, Saag KG, Bridges Jr SL, Akl EA, Bannuru RR, Sullivan MC, et al. 2015 American College of Rheumatology guideline for the treatment of rheumatoid arthritis. Arthritis Rheumatol. 2016;68(1):1–26.
[36] Nagaraj G, Mohammed MK, Shekargoftar M, Sasikumar P, Sakthivel P, Ravi G, et al. High-performance perovskite solar cells using the graphene quantum dot–modified SnO_2/ZnO photoelectrode. Mater Today Energy. 2021;22:100853.
[37] Suganya K, Maalmarugan J, Manikandan R, Nagaraj TS, Patel RP, Tamilarasi K, et al. Synthesis, studies of 2-benzyl-amino-4-p-tolyl-6, 7-di-hydro 5H-cyclo-penta–[b] pyridine-3 carbo-nitrile (BAPTDHC-PCN) crystals for optical, photonic and mechano-electronic uses. J Mater Sci Mater Electron. 2022;33(24):19320–30.
[38] Kambale RC, Shaikh PA, Bhosale CH, Rajpure KY, Kolekar YD. The effect of Mn substitution on the magnetic and dielectric properties of cobalt ferrite synthesized by an autocombustion route. Smart Mater Struct. 2009;18(11):115028.
[39] Joesna G, Saravanan P, Ferin RZ, Gunachitra T, Sankar D, Tamilselvan S, et al. Domestic microwave supported green synthesis of ZnO nanoparticles for electronic, mechano, rheological and frequency intensifying applications. J Mater Sci Mater Electron. 2022;33(17):14144–58.
[40] Senthilkumar N, Ganapathy M, Arulraj A, Meena M, Vimalan M, Potheher IV. Two step synthesis of ZnO/Ag and ZnO/Au core/shell

nanocomposites: structural, optical and electrical property analysis. J Alloy Compd. 2018;750:171–81.
[41] Kolaczkowski B, Thornton JW. Performance of maximum parsimony and likelihood phylogenetics when evolution is heterogeneous. Nature. 2004;431(7011):980–4.
[42] Saravanan P, SenthilKannan K, Divya R, Vimalan M, Tamilselvan S, Sankar D. A perspective approach towards appreciable size and cost-effective solar cell fabrication by synthesizing ZnO nanoparticles from Azadirachta indica leaves extract using domestic microwave oven. J Mater Sci: Mater Electron. 2020;31:4301–9.
[43] Maalmarugan J, Ferin RZ, Joesna G, Mustafa A, Mohamed MG, Bououdina M, et al. In situ grown ZnO nanoparticles using Begonia leaves–dielectric, magnetic, filter utility and tribological properties for mechano-electronic applications. Appl Phys A. 2022;128(3):217.
[44] Kumar NS, Ganapathy M, Sharmila S, Shankar M, Vimalan M, Potheher IV. ZnO/$Ni(OH)_2$ core-shell nanoparticles: synthesis, optical, electrical and photoacoustic property analysis. J Alloy Compd. 2017;703:624–32.
[45] Vasanth Winston X, Sankar D, SenthilKannan K, Vimalan M, Rajesh Kumar T. Gamma ray-irradiated induced effects on SCN ligand-based MMTC single crystals for optoelectronic applications synthesized by SR method. J Mater Sci Mater Electron. 2022;33:20616–30. doi: 10.1007/s10854-022-08873-8.
[46] Elashmawi IS, Alatawi NS, Elsayed NH. Preparation and characterization of polymer nanocomposites based on PVDF/PVC doped with graphene nanoparticles. Results Phys. 2017;7:636–40. doi: 10.1016/j.rinp.2017.01.022.
[47] Zhu L, Dong J, Jiang W, Yuan DD, Jiang H, Yan C, et al. Screening study on rheological behavior and phase transition point of polymer-containing fluids produced under the oil freezing point temperature. Open Chem. 2019;17(1):1442–8. doi: 10.1515/chem-2019-0158.